Journal of Materials Chemistry C

Accepted Manuscript

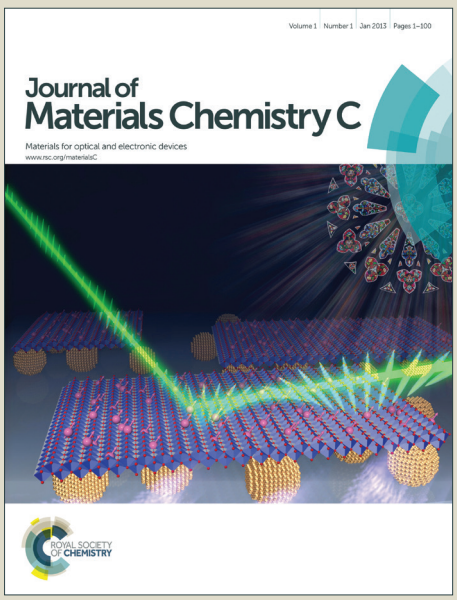

ROYAL SOCIETY OF CHEMISTRY

www.rsc.org/materialsC

Journal of Materials Chemistry C

PAPER

Solution-Processed Thermal-Stable Amorphous Films of Small Molecular Hole Injection/Transport Bi-functional Materials and its Application in High Efficient OLEDs

Received 00th January 20xx,
Accepted 00th January 20xx

DOI: 10.1039/x0xx00000x

www.rsc.org/

Xiaoming Zhao[a,b], Shirong Wang*[a,b], Jing You *[a,b], Yuteng Zhang [a,b] and Xianggao Li [a,b]

A series of novel triphenylamine-based small molecular hole transport materials (HTMs) are reported for solution processed organic light-emitting devices (OLEDs). The character of this series of HTMs, denoted as TPD(BTPA)$_n$ (n=1,2,4) is connecting the flexible moieties of butadiene bridged triphenylamine (BTPA) to the *N,N,N′,N′*-tetraphenyl-[1,1'-biphenyl]-4,4'-diamine(TPD). The glass transition temperature and crystallization temperature (T_g and T_c) showed an proportional relationship with the number of BTPA moieties. The T_g of TPD(BTPA)$_4$ can be up to 125.5℃, which is the higher than most of reported small molecular HTMs (T_g : 54℃-116℃). The TPD(BTPA)$_4$ spincoated film showed an outstanding thermal stability which maintained amorphous even annealed with 110℃, for 48 h. This indicated the break of planar molecular structure with BTPA moieties can suppress the intermolecular stacking. The solution processed OLEDs with 8-Hydroxyquinoline aluminum (Alq_3) as emission and electron transport layer showed high stability at high operation current (> 400 mA cm^{-2}). The OLED with TPD(BTPA)$_4$ achieved a maximum current efficiency of 5.83 cd A^{-1} (at the operation current density > 400 mA cm^{-2}), which is higher than the maximum current efficiency of most evaporation and solution processing OLEDs in identical structure.

Introduction

Organic light-emitting devices (OLEDs) are regarded as the next generation flat-panel displays because of advantages, such as portable, full colored, glare free, flexible, short response time, wider viewing angles *etc.*[1-3]

To date, there mainly are two issues need to be solved about small molecular OLEDs. First, the ultra-thin films in OLEDs are typically fabricated by vacuum evaporation (VE), which has demerits of high energy consuming, waste of materials and unfriendly to environment.[4] Secondly, the charge transfer and injection require homogeneous interface and layer, which means that the organic semiconductor film should be amorphous form.[5]

The first problem can be solved through solution processing techniques such as layer-by-layer spin coating and ink jet.[6] While, those techniques are mainly applied in the polymer materials. However, the research on structure-functional relationship of small molecular materials is more mature than the polymers.[7] Functional characteristics such as energy level of the polymers depends on not only the unit structure, but also the length of polymer chain which is not a constant.[8-10] It is believed that the design, synthesis and purification of small molecular materials are more convenient.

For the second problem, the crystallization of small molecular materials during film-forming in the solution process and operating at high temperature are main obstacles for its application in OLEDs.[11-14] The low glass transition and crystallization temperatures (T_g and T_c) lead to formation of polycrystalline in films resulting from thermal stress.[15] In the research reported by Douglas E Loy *et. al.*, the OLED with *N,N,N′,N′*-tetraphenyl-[1,1'-biphenyl]-4,4'-diamine (TPD) and *N,N′*-diphenyl-*N,N′*-bis-(1-naphthyl)-1,1′-biphenyl-4,4′-diamine (NPD) as HTL showed irreversible failure when heated at 100 and 110℃ due to crystallization.[16] As reported, the T_g and T_c of organic semiconductor are determined by the molecular structure. Larger molecular volume resulted in higher T_g.[17-19]

[a] *Department of Applied Chemistry,School of Chemical Engineering and Technology,Tianjin University, Tianjin 300072, China. E-mail: Youj1983@tju.edu.cn*
[b] *Collaborative Innovation Center of Chemical Science and Engineering (Tianjin), Tianjin 300072, China. E-mail: wangshirong@tju.edu.cn*
†Electronic Supplementary Information (ESI) available. See DOI: 10.1039/x0xx00000x

In this work, we designed and synthesized three new HTMs based on the TPD, which has a HOMO level of -5.30 eV and a T_g of 69℃.[20, 21] The TPD is modified with different numbers of 4-(penta-1,3-dien-1-yl)-N,N-diphenylaniline (BTPA) moieties (**Fig. 1**) to suppress the formation of crystal in film through reducing the molecular rigidity and breaking the molecular planarity. Comparing with triphenylamine, BTPA moieties can be introduced simply with witting-honor reaction, which reaction condition is much milder than Ullmann reaction or carbon-carbon coupling reaction.[22, 23] In addition, the BTPA moiety has larger volume than triphenylamine, which are benefit for suppressing intermolecular stacking in solid states. With considering above reasons, we chose BTPA moieties to modify the TPD The molecular structures are shown in **Fig. 1** and denoted as TPD(BTPA)$_n$ (n=1,2,4). The crystallization during the spin-coating film forming process and the thermal stability of these films are investigated by X-ray diffraction (XRD), attenuated total reflectance fourier transform infrared spectroscopy (ATR-FTIR) and differential scanning calorimetry (DSC) measurements. The thermal stability increases gradually with the increasing number of BTPA moieties connected to the TPD. Notably, the spin-coating film of TPD(BTPA)$_4$ can maintain amorphous even after annealed at 110 ^{o}C for 48 h. At present, the reported HTM films crystallized with annealing at < 95 ^{o}C for < 2 h, such as *N,N,N′,N′*-tetraphenylbenzidine (TPB), *N,N,N′,N′*-tetra-p-tolyl-benzidine (TTB), *N,N′*-di(naphthalene-1-yl)-*N,N′*-diphenyl-benzidine (NPB), 9,10-(2-naphthyl)anthracene (AND), 1,4-bis(phenyl-m-tolylamino) biphenyl (TPD), 1,4-bis(benzothiazole-vinyl) benzene (BT) *et. al.*.[24-30]

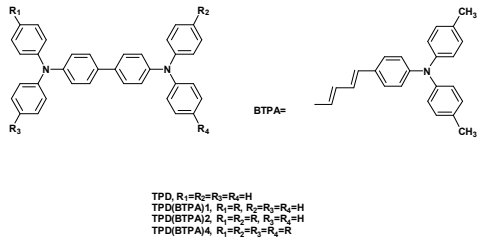

Fig. 1 Molecular structures of TPD(BTPA)$_n$ compounds

The hole transport properties of as-synthesized HTMs are evaluated in the solution processed OLEDs with the structure of ITO/HTMs/Alq_3/LiF:Al. This structure with small molecular HTMs (molecular weight < 6000 g mol^{-1}) has been reported by many groups with maximum current efficiency (CE_{max}) smaller than 5.7 cd A^{-1}, which are listed in **Table 5.**[6, 11, 31-44]

In this work, the Device-TPD(BTPA)$_4$ can exhibit the CE_{max} of 5.83 cd A^{-1} at the operation current intensity larger than 400 mA cm^{-2}. This CE_{max} is highest among the reported small molecular OLED (molecular weight < 6000 g mol^{-1}) in identical structure no matter fabricated with evaporation or solution processing.[6, 11, 31-44]

Results and Discussions

Synthesis and Characterizations

The TPD(BTPA)$_n$ (n=1,2,4) are synthesized by formylation and Wittig-Honor reactions starting with TPD (**Scheme 1**).[45]

The BTPA moieties were synthesized from 4-(di-p-tolylamino)benzaldehyde (Me-TPA-CHO) by formylation and Wittig-Honor reactions. The total yield of 3-(4-(di-p-tolylamino)phenyl)prop-2-en-1-ol (Me-TPA-CH=CH-CH_2OH) was 92.0%. The aldehybe groups were introduced on the TPD with different numbers. Then the BTPA moieties were introduced on the TPD(CHO)$_n$ (n=1,2,4) by Witting-Honor reaction. The yields were 72.3% (TPD(BTPA)$_1$), 68.2% (TPD(BTPA)$_2$) and 63.4% (TPD(BTPA)$_3$), respectively. The TPD(BTPA)$_n$(n=1,2,4) compounds are soluble in methylbenzene, chlorobenzene, tetrahydrofuran and chloroform, *etc*. The well-defined structures of all novel compounds are adequately verified by ^{1}H NMR, mass spectrometry and IR spectroscopy (see details in the **ESI**).

The decomposition temperatures (T_d, which correspond to 5% weight loss) of TPD(BTPA)$_n$ (n=0-4), recorded by thermal gravity analysis (TGA), are 411℃(TPD(BTPA)$_1$), 425℃ (TPD(BTPA)$_2$), and 448℃(TPD(BTPA)$_4$), respectively (**Fig. S10**, Supporting Information). With the increase of ***n*** in TPD(BTPA)$_n$, the T_d of as-synthesized HTMs increase gradually.

Scheme 1 Synthetic routes of TPD(BTPA)$_n$ (n=1,2,4).

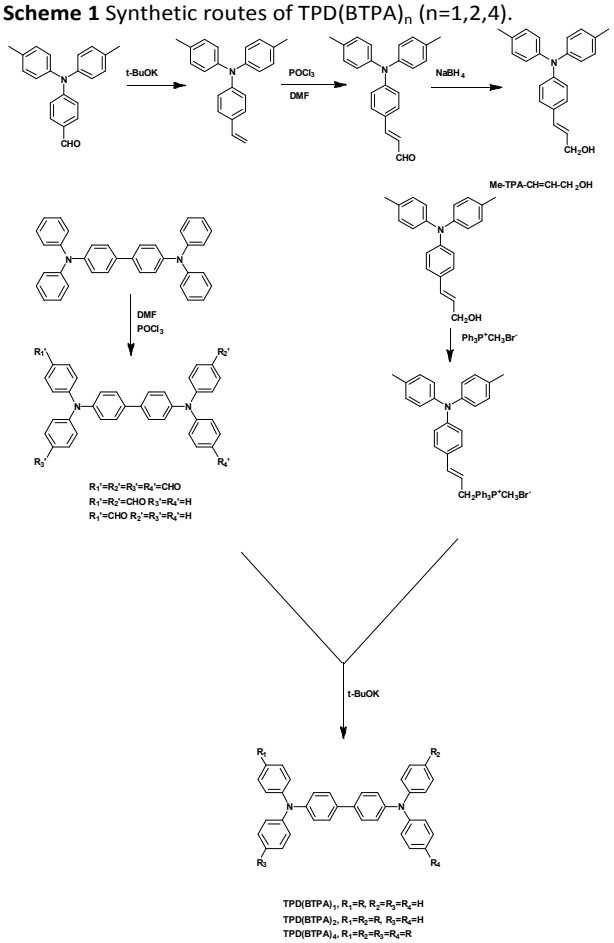

Photophysical and Electrochemical Properties

UV-vis absorption spectra of TPD(BTPA)$_n$(n=0,1,2,4) are shown in **Fig. 2** and relative data are summarized in **Table 1**. Cyclic voltammograms of TPD(BTPA)$_n$ (n=0,1,2,4) are shown in **Fig. S11** (**ESI**).

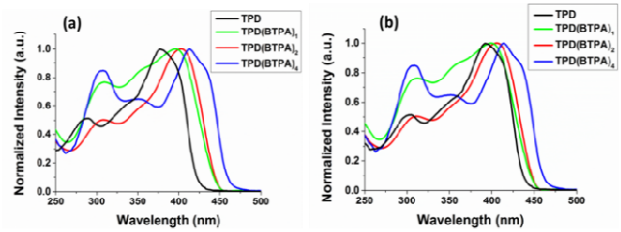

Fig. 2 Normalized absorption spectra of TPD(BTPA)$_n$ (n=0,1,2,4) in chlorobenzene solution with concentration of 1.0×10^{-5} M (a) and spincoating films (b).

As shown in the **Fig. 2a**, the absorption peaks in the wavelength region 280-310 nm can be assigned to the n-π transition of the TPA moiety. The absorption peaks in the region 375-450 nm can be assigned to the intramolecular charge transfer (ICT) of π-π* transition. There is an obvious red shift of ICT peaks and decrease of energy gap (E_g) with the increasing number of BTPA moiety. The absorption spectrum of each TPD(BTPA)$_n$ compound in solid state film reveals no red-shift compared to that in chlorobenzene solution, indicating that no significant aggregation or crystallization occurs in the films of TPD(BTPA)$_n$(n=1,2,4).[46]

As shown in **Table 1**, with the increase of number ***n*** in TPD(BTPA)$_n$, the HOMO level increases from -5.30eV(TPD(BTPA)$_1$) to -5.12eV(TPD(BTPA)$_4$), which exhibits the HOMO level can be modified through changing the number of BTPA moiety. The HOMO level of TPD(BTPA)$_4$ matches the work function of ITO (-4.80 eV) quite well, which could benefit the charge injection without the assistant of the normally-used hole injection layer (HIL) poly(3,4-ethylene-dioxythiophene) poly(styrene sulfonate) (PEDOT:PSS).[47]

Thermal Properties of TPD(BTPA)$_n$

The thermal properties of TPD(BTPA)$_n$ (n=0,1,2,4) are investigated by the differential scanning calorimetry(DSC)

As shown in **Fig. 3**, the T_g, T_c and T_m of TPD(BTPA)$_n$ (n=0,1,2,4) increase gradually with the increasing number of BTPA moieties (**n**). The T_g and T_c of TPD(BTPA)$_4$ are higher than most of common used small molecular HTMs.[29-34] The corresponding enthalpies of crystallization are 41.51 Jg^{-1}(TPD), 44.26 Jg^{-1}(TPD(BTPA)$_1$), 31.5 Jg^{-1}(TPD(BTPA)$_2$) and 28.26 Jg^{-1}(TPD(BTPA)$_4$), respectively. This indicates that the TPD and TPD(BTPA)$_1$ have higher crystallization tendency than TPD(BTPA)$_2$ and TPD(BTPA)$_4$.[6] Apparently, the BTPA moieties showed a capability for improving thermal stability, while only one BTPA moiety was not enough for changing crystallization property noticeably.

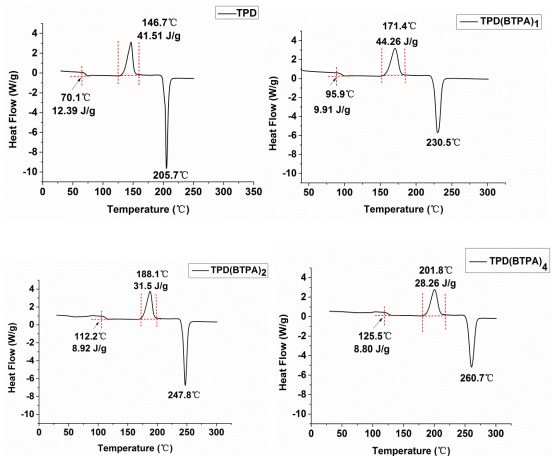

Fig. 3 DSC curves of TPD(BTPA)$_n$ (n=0,1,2,4) selected from the heating of second loop.

Table 1. The optical, thermal properties and energy levels of TPD(BTPA)$_n$ (n=0,1,2,4)

	T_d [a] (°C)	T_g [b] (°C)	T_c [b] (°C)	T_m [b] (°C)	λ_{ITC} [c] (nm)	E_g [d] (eV)	HOMO [e] (eV)	LUMO [e] (eV)
TPD	375	70.1	146.7	205.7	391	3.10	-5.30	-2.20
TPD(BTPA)$_1$	411	95.9	17.4	230.5	399	2.94	-5.21	-2.27
TPD(BTPA)$_2$	425	112.2	188.1	247.8	407	2.82	-5.16	-2.34
TPD(BTPA)$_4$	448	125.5	201.8	260.7	415	2.73	-5.12	-2.39

[a] Measured by TGA at a heating rate of 10 °C min^{-1} under nitrogen atmosphere. [b] T_g glass transition temperature, T_c crystallization temperature, and T_m melt point measured by DSC according to the heat-cool-heat procedure (Fig. 3). [c] Intramolecular charge transfer peak of thin films. [d] Optical energy gaps calculated from the absorption thresholds from UV-Vis absorption spectra of chlorobezene solutions (1.0×10^{-5} M). [e] Measured by cyclic voltammetry.

Crystallization of Spincoated Films

The amorphous films can improve charge injection and transfer between different layers.[48-50] It is important to find out when the crystallization occurs. Therefore, we measured the crystallinity of spincoated films before and after annealing though X-Ray Diffraction(XRD) and Attenuated Total Reflectance-Fourier Transformed Infrared Spectroscopy (ATR-FTIR).

The XRD spectra of TPD(BTPA)$_n$ films are shown in **Fig. 4**. When the TPD(BTPA)$_n$ (n=0,1,2,4) were spincoated on the ITO substrate, the XRD patterns in the region of 0<2θ<5.0° were same as that of ITO substrate, which indicating that all these spincoated films were amorphous. The diffraction peaks ($2\vartheta \approx 1.5^{o}$) can be observed in TPD and TPD(BTPA)$_1$ when these films were annealed at 70℃ for 24 h. The diffraction peaks ($2\vartheta \approx 1.5^{o}$) in TPD(BTPA)$_2$ and TPD(BTPA)$_4$ films appeared at annealing temperature of 100℃and 120℃, respectively. As shown in **Fig. 5(B)**, for the TPD(BTPA)$_4$ film, the XRD pattern maintained unchanged even annealed at 110℃ for 48 h.

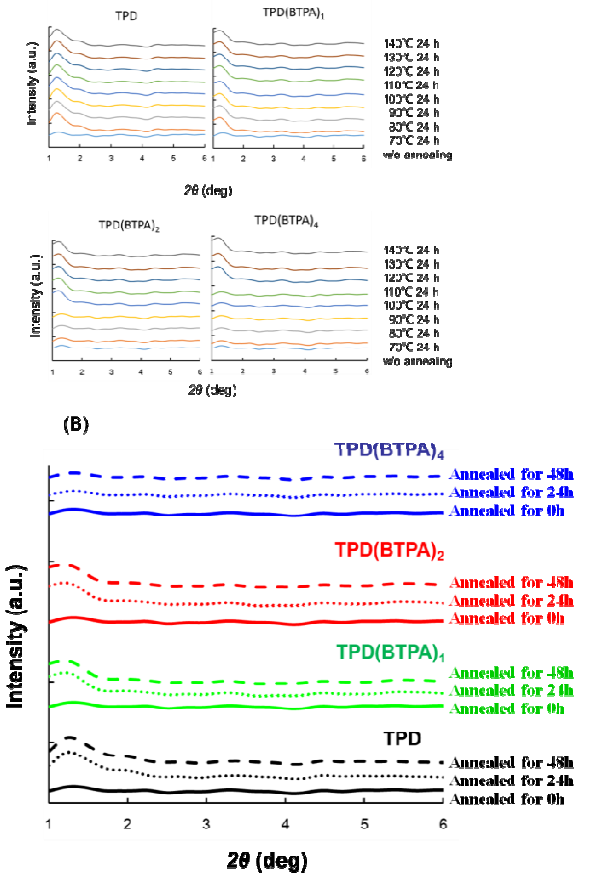

Fig. 4 X-ray diffraction patterns of films on ITO glass substrate annealed from 70-140 ℃ for 24 h (a); annealed at 110℃ for 0-48 h(b)

The crystallinity were confirmed directly by ATR-FTIR measurement.[51] As shown in **Fig. 5**, for spincoated films of TPD and TPD(BTPA)$_1$, a broad band in the wavenumber region of 900-1200 cm^{-1}, and a small band in the wavenumber region of 700-800 cm^{-1} generated after annealing. The broad band can be assigned to the in-plane vibration of benzene.[52] This phenomenon generate from the change of optical property after crystallization. The change of ATR-FTIR spectra for TPD(BTPA)$_2$ and TPD(BTPA)$_4$ films before and after annealing at 100℃ are unobvious, which mean the TPD(BTPA)$_2$ and TPD(BTPA)$_4$ films maintained amorphous. For most of reported small molecular HTMs, such as TPB, TTB, NPB, AND, TPD and BT, these films cannot maintain amorphous form with annealing > 80℃ less than 2 h.[29-34]

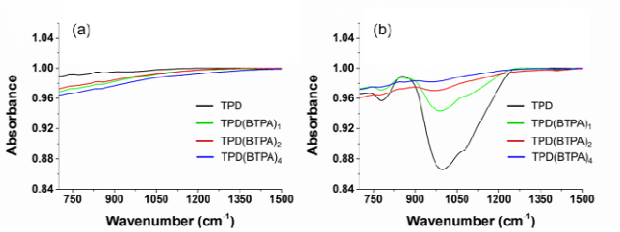

Fig.5 ATR-FTIR spectra of TPD compounds before(a) and after annealing(b).

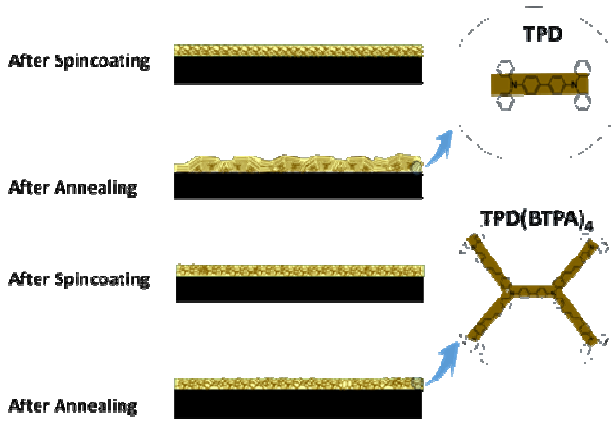

Fig. 6 Crystallization process in spincoated films.

All the results above indicate that the crystallization capability is suppressed with BTPA moieties. The crystallization process does not happen during spincoating process. Instead, it occurs after the film-forming process. The possible process is shown in **Fig. 6**.

All the spincoated films are amorphous before annealing. As shown in **Fig. 6**, we discuss the two extreme situations: TPD (crystalline) and TPD(BTPA)$_4$ (amorphous). In the case of TPD, after spincoating the TPD molecules deposit on the substrate randomly and the TPD film is amorphous accordingly. While, the TPD molecule tends to stack because of its planarity molecular structure, low T_g and T_c, as well as the large change of enthalpies after crystallization. Then, the orientated aggregation (crystallization) occurs, which will break the homogenous TPD films.

In the case of TPD(BTPA)$_4$, the film maintains amorphous after annealing. Compared with TPD, the molecular structure of TPD(BTPA)$_4$ is nonplanar. In addition, the TPD(BTPA)$_4$ has higher T_g, T_c and smaller change of enthalpies after crystallization. These prevent the orientated aggregation (crystallization) in TPD(BTPA)$_4$ after annealing. The crystallization property of TPD(BTPA)$_1$ and TPD(BTPA)$_2$ should be between that of TPD and TPD(BTPA)$_4$.

Molecular Geometry

One of the most important roles of BTPA moiety is breaking the planarity of TPD. In this work, the molecular geometry was applied to estimate the change of planarity. First, the molecular geometries of TPD(BTPA)$_n$ (n=0,1,2,4) were optimized with Gaussian 03 program.[53] Then the cartesian coordinates of all the atoms in each molecule were obtained from above step. We put the molecule into a regular hexahedron as shown in **Fig. 7**.

The ***L, W, H*** and volume of regular hexahedron are listed in **Table 2**. Apparently, the TPD molecule is much close to a plate. With the increasing BTPA moieties, the molecules of TPD(BTPA)$_n$ (n=1,2,4) are approach to cubes. This indicated that, beside increasing the molecular volume, the BTPA moieties can break the molecular planar effectively. This change of molecular geometry greatly affect the thermal stability of TPD(BTPA)$_n$, which leads to the amorphous films of TPD(BTPA)$_4$ even after annealing at 110 °C for 48 h.

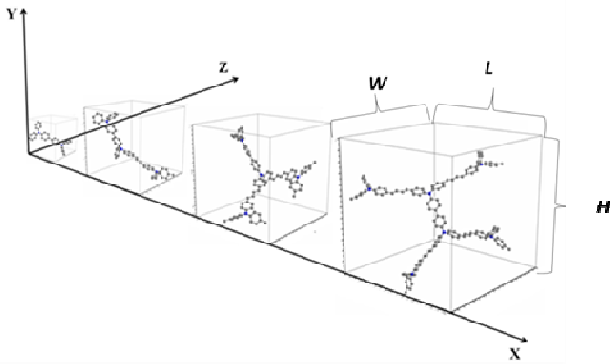

Fig. 7 Molecular geometry of TPD(BTPA)$_n$ (n=0,1,2,4) in a regular hexahedron with length, width and height of *L, W* and *H*, respectively.

Table 2. Geometry Parameters of TPD(BTPA)$_n$ (n=0, 1, 2, 4)

	L[a)]	***W***.[a)]	***H***[a)]	Volume[b)]	***L:W:H***[c)]
TPD	15	6	16	1440	2.5:1.0:2.7
TPD(BTPA)$_1$	14	16	25	5600	1.0:1.1:1.8
TPD(BTPA)$_2$	14	21	36	10584	1.0:1.5:2.6
TPD(BTPA)$_4$	38	25	36	34200	1.52:1.0:1.44

[a)] Estimated by the cartesian coordinates of all the atoms after geometry optimized with Gaussian 03. [b)] Volume = ***L*×*W*×*H***. [c)] Normalized with minimum value of ***L***,***W*** and ***H***; all the units are a.u..

Application in OLEDs

One role of BTPA moiety is increasing the molecular volume to suppress crystallization in films and improve the thermal stability. Another role is increasing the molecular conjugation by introducing the butadiene units. As discussed above, with the increasing number of BTPA moieties, the HOMO levels of as-synthesized HTMs slightly increases.

As the HOMO levels of TPD(BTPA)$_n$ (n=0-4) are in the range of -5.12～-5.40 eV which are very close to the HOMO level of commonly-used hole injection material PEDOT:PSS (-5.00 eV), [54] we fabricate double-layer OLEDs using TPD(BTPA)$_n$ as hole injection/transport double-functional layers, Alq_3 as electron transport and emission layers, with the device structure: ITO/TPD(BTPA)$_n$ (200 nm)/Alq_3 (70 nm)/LiF (0.5 nm)/Al (120 nm). The current-voltage-luminance (*J-V-L*) characteristic curves and *LE-J* of these OLEDs are shown in **Fig. 8**, the parameters are listed in **Table 3**.

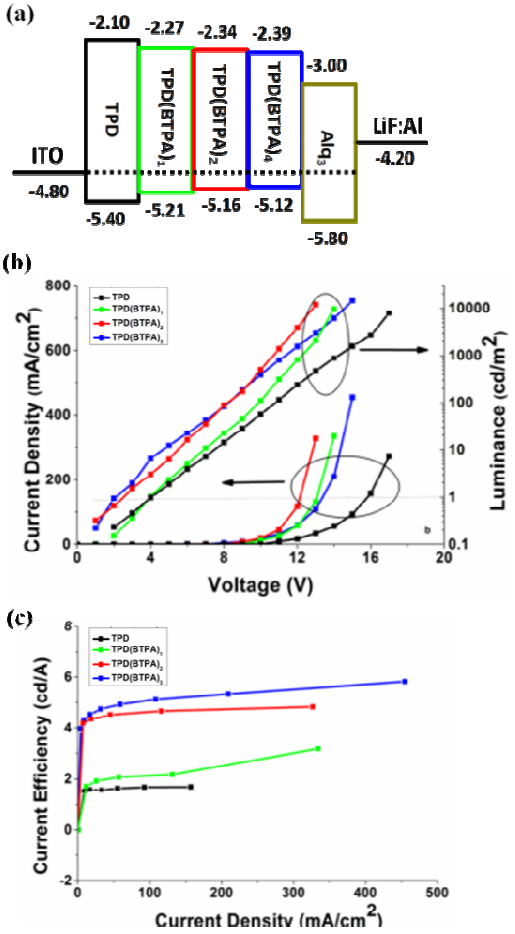

Fig. 8 OLED structures(a), *J-V-L* curves (b) and *J-η* curves(c)

As shown in **Fig. 8(b)** and **Table 3**, the ture-on voltage(V_{on}) of Device-TPD and Device-TPD(BTPA)$_1$ are the same, despite the HOMO level of TPD(BTPA)$_1$ (-5.21eV) is much closer to the work function of ITO (-4.80 eV) than TPD (-5.40 eV). However, compared to Device-TPD, the V_{on} reduces 28% (Device-TPD(BTPA)$_2$) and 38% (Device-TPD(BTPA)$_4$). This indicated the smaller difference between ITO work function and HOMO level of TPD(BTPA)$_n$ are beneficial to hole injection.

Table 3. Electroluminescence characteristics of OLEDs

Device	V_{on} [a] (V)	L_{max} [b] (cd m^{-2})	CD [b] (mA cm^{-2})	CE [c] (cd A^{-1})	μ_h [d] (×10^{-5} cm V^{-1}S^{-1})
TPD	5.0	8152 (17.0 V)	272	2.16	140
TPD(BTPA)$_1$	5.0	9590 (13.9 V)	334	3.17	24
TPD(BTPA)$_2$	3.6	12281 (13.1 V)	327	4.83	15
TPD(BTPA)$_4$	3.1	14446 (15.2 V)	455	5.83	9

[a] Turn-on voltage:the voltage at the brightness of 1 cd m^{-2}; [b] Maximum brightness and corresponding voltage in the bracket; [c] Maximum current efficiency; [d] Measured in hole-only devices (structure: ITO/HTMs (~1 μm)/Al (120 nm)). Hole mobilities are determined by time-of-fight (TOF) method[29], details see **ESI Fig. S12**.

From the **Table 3**, compared with Device-TPD, the maximum brightness (L_{max}) increase 20% (Device-TPD(BTPA)$_1$), 50% (Device-TPD(BTPA)$_2$) and 80% (Device-TPD(BTPA)$_4$); the maximum current efficiency (CE_{max}) increase 50%, 120% and 170% , respectively. The LUMO levels of TPD(BTPA)$_n$ (n=0-4) are in the range of -2.10~-2.39 eV, which are higher than the LUMO level of Alq$_3$ and it means that the TPD(BTPA)$_n$ (n=0-4) layer can play the role of electron blocking.

Hole mobilities of TPD(BTPA)$_n$ (n=0,1,2,4) decreased with increasing number of BTPA moieties n. This mainly result from the suppression of crystallization by BTPA moieties. The electron mobility (μ_e) of Alq$_3$ was reported to be ~1.1-2.3×10^{-5} cm V^{-1}S^{-1}.[29] The equilibrium of electron and hole transport in device-TPD(BTPA)$_4$ resulted higher CE than other OLEDs.

The most interesting phenomenon is that the *CE* increases with higher operation current in the Device-TPD(BTPA)$_1$, Device-TPD(BTPA)$_2$, and Device-TPD(BTPA)$_4$. This should result from the outstanding thermal stability of the TPD(BTPA)$_n$ (n=2,4) films which can maintain amorphous even at high operation current.

To further investigate the hole injection/transport properties of TPD(BTPA)$_4$, we compare the performance of OLEDs with and without PEDOT:PSS layer, which are denoted as Device-PP-TPD(BTPA)$_4$ (structure: ITO/PEDOT:PSS (100nm)/TPD(BTPA)$_4$ (200 nm)/Alq$_3$ (70 nm)/LiF (0.5 nm)/Al (120 nm)and Device-TPD(BTPA)$_4$ (device structure: ITO/TPD(BTPA)$_4$ (200 nm)/Alq$_3$ (70 nm)/LiF (0.5 nm)/Al (120 nm)), respectively. The device structures, current-voltage-luminance (*J-V-L*) characteristic curves and current-efficiency (*J-* η) curves are shown in **Fig. 9**, parameters are listed in **Table 4**.

As reported, the PEDOT:PSS normally applied to improve hole injection because of its HOMO level closing to the work function of ITO. However, the Device-PP-TPD(BTPA)$_4$ shows a higher V_{on} (3.1 V) and a lower CE_{max} (4.48 cd A^{-1}) than Device-TPD(BTPA)$_4$. From **Fig. 9 (c)**, it can be found that with the increasing current intensity, the efficiency of the Device-PP-TPD(BTPA)$_4$ reduces obviously. On the contrary, the Device- TPD(BTPA)$_4$ remains stable.

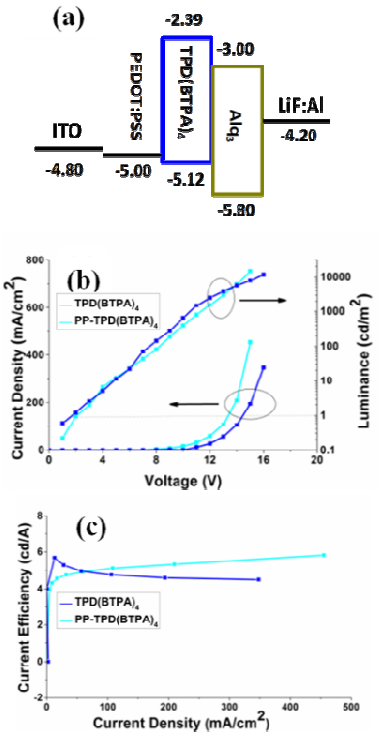

Fig. 9 OLED structures(a), *J-V-L* curves(b) and *J-* η curves(c)

Table 4. Electroluminscence characteristics of OLEDs

Device	V_{on} [a] (V)	L_{max} [b] (cd m^{-2})	CD [c] (mA cm^{-2})	CE [d] (cd A^{-1})
TPD(BTPA)$_4$ [e]	3.1	14446 (15.2)	455	5.83
PP- TPD(BTPA)$_4$ [f]	3.8	12280 (16.1)	348	4.48

[a] Turn-on voltage:the voltage at the brightness of 1 cd m^{-2}; [b] Maximum brightness; [c] Current efficiency at the maximum brightness; [d] Maximum current efficiency;

It has been reported that during spin-coating the acidity of PEDOT:PSS colloidal solution can corrode ITO to dissolve some In^{3+}. The In^{3+} will make the PEDOT:PSS interface unstable and obstruct the hole injection, which will diffuse to emitting layer to form a quenching center when devices operating at high current. This should be the reason for decrease of CE_{max} at higher current density in Device-PP-TPD(BTPA)$_4$.[55-59]

In Device-TPD(BTPA)$_4$, both the performance and the stability at high current density of OLEDs have been improved. The improvement of OLED performance at high operation currents should be result from the combine effects of outstanding thermal stability of hole transport layer and balance of electron-hole transporting in device. This confirms that the TPD(BTPA)$_n$ (n>1) can be applied as hole injection/transport di-functional material to improve the performance and stability of OLEDs, as well as simplify the fabrication process of solution-processing OLEDs.

The HTMs applied in solution-processing OLEDs with identical structure are reported. [6, 11, 31-44] The molecular formula (MF), molecular weight (MW), HOMO level, LUMO level, energy gap of reported HTMs and corresponding parameters of OLEDs are listed in **Table 5**. All the molecular structure are listed in **ESI Fig. S13**.

Table 5. Reported HTMs for solution-processing OLEDs with identical structure

Componds	MF	MW	HOMO (eV)	LUMO (eV)	E_g (eV)	Device Structure	V_{on} (V)	CE (cd A^{-1})	$J_{90\%}$ (mA cm^{-2})
[a]DT2 [6]	$C_{432}H_{300}N_{22}$	5799	-5.22	-2.60	2.62	ITO/PEDOT:PSS/DT2/Alq3/LiF:Al	2.9	2.36	5
[a]G3F2[34]	$C_{242}H_{212}N_{14}$	3316	-5.4	-2.19	3.21	ITO/PEDOT:PSS/G3F2/Alq3/LiF:Al	2.6	5.63	123
[a]TPD(BTPA)$_4$[c]	$C_{123}H_{112}N_6$	1782	-5.12	-2.39	2.73	ITO/TPD(BTPA)$_4$/Alq3/LiF:Al	3.1	**5.83**	Unobservable
						ITO/PEDOT:PSS/TPD(BTPA)$_4$/Alq3/LiF:Al	3.8	4.48	168
[a]G3C[36]	$C_{97}H_{77}N_7$	1341	-5.37	-2.01	3.36	ITO/PEDOT:PSS/G3C/Alq3/LiF:Al	3	5.11	103
[a]T4C[35]	$C_{96}H_{85}N_5$	1309	-5.15	-1.91	3.24	ITO/PEDOT:PSS/T4C/Alq3/LiF:Al	2.5	5.07	160
[a]FC[37]	$C_{85}H_{97}N_3$	1161	-5.21	-2.39	2.82	ITO/PEDOT:PSS/FC/Alq3/LiF:Al	5.6	3.2	155
[b]TECEB [31]	$C_{54}H_{45}N_3$	735	-5.20	-2.40	2.80	ITO/TECEB/Alq3/Mg:Ag	3.5	3.27	120
[b]FTPD7 [30]	$C_{53}H_{44}N_2$	708	-5.80	-2.12	3.68	ITO/FTPD7/Alq3/LiF:Al	6.5	2.18	\
[a]TPD [11]	$C_{36}H_{28}N_2$	488	-5.40	-2.10	3.30	ITO/TPD/Alq3/LiF:Al	2.0	3.67	200

[a] Spin-coated HTMs; [b] Vacuum-deposited HTMs ; [c] As-synthesized HTM in this work

As shown in **Table 5**, the Device-TPD(BTPA)$_4$ shows the highest CE_{max} which is far beyond other reported small molecular HTMs (Mw< 6000) with identical structure no matter fabircated by vacuum deposition or spin-coated. [6, 11, 31-44] In addition, the efficiency roll-off is unobservable in device applying TPD(BTPA)$_n$ (n=1,2,4) as hole transport/injection bi-functional material, which confirmed the outstanding operation stability even at large operation current. At present, only the 1,2,3,4,5,6-hexakis(9,9-dihexyl-9H-fluoren-2-yl)benzene T3(CE_{max} =6.45 cd A^{-1}) showed slightly higher efficiency than Device-TPD(BTPA)$_4$.[40] However, the MW of T3 is much larger than TPD(BTPA)$_4$ (>4 times). Not a mention the V_{on} of Device-T3 (5.5 V) is much higher than Device-TPD(BTPA)$_4$ (3.1 V).[40]

Conclusions

In this work, the novel HTMs TPD(BTPA)$_n$ (n=1,2,4) have been designed and synthesized. The BTPA moieties are introduced into TPD to improve thermal stability and suppress crystallization in spincoated films. The thermal stability of TPD(BTPA)$_n$ (n=0,1,2,4) have been investigated by DSC, which shows gradual increases of T_g, T_c and T_m with the increasing number of TBPA moieties. The spincoated film of TPD(BTPA)$_4$ maintained amorphous form even with 110℃, 48 h annealing which confirmed by XRD and ATR-FTIR. The OLEDs with TPD(BTPA)$_n$ (n=0,1,2,4) as HIL and HTL showed an improvement of performance with increasing the number of TBPA moieties. The BTPA moieties can improve the stability of OLED operated with high current. The OLED with TPD(BTPA)$_4$ showed the highest CE_{max} compared with reported small molecular (Mw<6000) HTMs with identical structure no mater solution processing or vacuum deposition.

Acknowledgements

We are grateful to the National High Technology Research and Development Program of China (863 Program, 2015AA033402) and the Key Technologies R&D Rrogram of Tianjin (13ZCZDGX00900) for financial support of this research.

Notes and references

1. B. Richter, U. Vogel, R. Herold, F. Karsten, B. Stephan, L. Kroker and J. Baumgarten, *Solid-State Circuits*

Conference Digest of Technical Papers (ISSCC), 2011 IEEE International, 2011, 314 - 316.

2. O. Prache, *Displays*, 2001, **22**, 49-56.

3. R. Martins, V. Shaoulov, Y. G. Ha and J. Rolland, *Opt Express*, 2007, **15**, 14530-14538.

4. Y. Shirota, *J Mater Chem*, 2005, **15**, 75-93.

5. D. Yokoyama, *J Mater Chem*, 2011, **21**, 19187-19202.

6. C. Li, Y. J. Chen, Y. Zhao, H. F. Wang, W. Zhang, Y. W. Li, X. M. Yang, C. Q. Ma, L. W. Chen, X. L. Zhu and Y. F. Tu, *Nanoscale*, 2013, **5**, 9536-9540.

7. Z. A. Li, T. L. Ye, S. Tang, C. Wang, D. G. Ma and Z. Li, *J Mater Chem C*, 2015, **3**, 2016-2023.

8. Z. K. Fan, N. Q. Li, Y. W. Quan, Q. M. Chen, S. H. Ye, Q. L. Fan, W. Huang and H. Xu, *J Mater Chem C*, 2014, **2**, 9754-9759.

9. F. Villani, P. Vacca, G. Nenna, O. Valentino, G. Burrasca, T. Fasolino, C. Minarini and D. della Sala, *J Phys Chem C*, 2009, **113**, 13398-13402.

10. H. Gorter, M. J. J. Coenen, M. W. L. Slaats, M. Ren, W. Lu, C. J. Kuijpers and W. A. Groen, *Thin Solid Films*, 2013, **532**, 11-15.

11. B. Geffroy, P. Le Roy and C. Prat, *Polym Int*, 2006, **55**, 572-582.

12. N. K. Adachi and N. Tamoto, *Applied physics letters*, 1995, **66**, 2679-2681.

13. J. W. Kingsley, P. P. Marchisio, H. Yi, A. Iraqi, C. J. Kinane, S. Langridge, R. L. Thompson, A. J. Cadby, A. J. Pearson, D. G. Lidzey, R. A. L. Jones and A. J. Parnell, *Sci Rep*, 2014, **4**, 5286.

14. Z. Y. Xiao, K. Sun, J. Subbiah, T. S. Qin, S. R. Lu, B. Purushothaman, D. J. Jones, A. B. Holmes and W. W. H. Wong, *Polym Chem*, 2015, **6**, 2312-2318.

15. G. L. Gibson, D. Gao, A. A. Jahnke, J. Sun, A. J. Tilley and D. S. Seferos, *J Mater Chem A*, 2014, **2**, 14468-14480.

16. D. E. Loy, B. E. Koene and M. E. Thompson, *Adv Funct Mater*, 2002, **12**, 245-249.

17. S. Feng, L. Duan, L. D. Hou, J. Qiao, D. Q. Zhang, G. F. Dong, L. D. Wang and Y. Qiu, *J Phys Chem C*, 2011, **115**, 14278-14284.

18. T. T. Adachi C and Saito S, *Applied Physics Letters*, 1990, **56**, 799-801.

19. M. Nagai and H. Nozoye, *J Electrochem Soc*, 2007, **154**, J239-J245.

20. T. Y. Tokito S, *Appl Phys Lett*, 1995, **66**, 673-675.

21. P. F. Smith, P. Gerroir, S. Xie, A. M. Hor, Z. Popovic and M. L. Hair, *Langmuir*, 1998, **14**, 5946-5950.

22. H. Zhao, C. Tanjutco and S. Thayumanavan, *Tetrahedron Lett*, 2001, **42**, 4421-4424.

23. Z. Ge, T. Hayakawa and S. Ando, *Adv Funct Mater*, 2008, **18**, 584-590.

24. M. Thelakkat, *Macromol Mater Eng*, 2002, **287**, 442-461.

25. P. Wei, X. D. Bi, Z. Wu and Z. Xu, *Org Lett*, 2005, **7**, 3199-3202.

26. H. Choi, S. Park, S. Paek, P. Ekanayake, M. K. Nazeeruddin and J. Ko, *J Mater Chem A*, 2014, **2**, 19136-19140.

27. J. C. S. Costa and L. M. N. B. F. Santos, *J Phys Chem C*, 2013, **117**, 10919-10928.

28. B. L. Groenendaal, F. Jonas, D. Freitag, H. Pielartzik and J. R. Reynolds, *Adv Mater*, 2000, **12**, 481-494.

29. X. S. Ma, S. R. Wang, X. G. Li and Y. Xiao, *Org Electron*, 2014, **15**, 1876-1883.

30. F. X. Wang, X. F. Qiao, T. Xiong and D. G. Ma, *Org Electron*, 2008, **9**, 985-993.

31. S. W. Wen, M. T. Lee and C. H. Chen, *J Disp Technol*, 2005, **1**, 90-99.

32. J. D. You, S. R. Tseng, H. F. Meng, F. W. Yen, I. F. Lin and S. F. Horng, *Org Electron*, 2009, **10**, 1610-1614.

33. J. Cui, Q. L. Huang, J. C. G. Veinot, H. Yan, Q. W. Wang, G. R. Hutchison, A. G. Richter, G. Evmenenko, P. Dutta and T. J. Marks, *Langmuir*, 2002, **18**, 9958-9970.

34. J. R. Gong, L. J. Wan, S. B. Lei, C. L. Bai, X. H. Zhang and S. T. Lee, *J Phys Chem B*, 2005, **109**, 1675-1682.

35. O. H. Kuwabara Y and Inada H, *Adv Mater*, 1994, **6**, 677-679.

36. M. Kimura, S. Kuwano, Y. Sawaki, H. Fujikawa, K. Noda, Y. Taga and K. Takagi, *J Mater Chem*, 2005, **15**, 2393-2398.

37. O. T. Okutsu S and Tamano M,*Electron Devices*, 1997, **44**, 1302-1306.

38. J. Y. Li, D. Liu, Y. Q. Li, C. S. Lee, H. L. Kwong and S. T. Lee, *Chem Mater*, 2005, **17**, 1208-1212.

39. Y. L. C. C. C. Cheng, F. H. Chang, D. J. Lee, *Nano Energy*, 2015, **13**, 1-8.

40. Y. Zou, J. H. Zou, T. L. Ye, H. Li, C. L. Yang, H. B. Wu, D. G. Ma, J. G. Qin and Y. Cao, *Adv Funct Mater*, 2013, **23**, 1781-1788.

41. P. Moonsin, N. Prachumrak, S. Namuangruk, S. Jungsuttiwong, T. Keawin, T. Sudyoadsuk and V. Promarak, *J Mater Chem C*, 2014, **2**, 5540-5552.

42. P. Kochapradist, N. Prachumrak, R. Tarsang, T. Keawin, S. Jungsuttiwong, T. Sudyoadsuk and V. Promarak, *Tetrahedron Lett*, 2013, **54**, 3683-3687.

43. N. Prachumrak, S. Pansay, S. Namuangruk, T. Kaewin, S. Jungsuttiwong, T. Sudyoadsuk and V. Promarak, *Eur J Org Chem*, 2013, **2013**, 6619-6628.

44. C. S. Wu, S. W. Fang and Y. Chen, *Phys Chem Chem Phys*, 2013, **15**, 15121-15127.

45. W. Z. Gao, S. R. Wang, Y. Xiao and X. G. Li, *Dyes Pigments*, 2013, **97**, 92-99.

46. C. Y. Jiang, X. W. Sun, D. W. Zhao, A. K. K. Kyaw and Y. N. Li, *Sol Energ Mat Sol C*, 2010, **94**, 1618-1621.

47. Z. Q. Gao, W. Y. Lai, T. C. Wong, C. S. Lee, I. Bello and S. T. Lee, *Appl Phys Lett*, 1999, **74**, 3269-3271.

48. B. E. Koene, D. E. Loy and M. E. Thompson, *Chem Mater*, 1998, **10**, 2235-2250.

49. T. Kato, T. Mori and T. Mizutani, *Thin Solid Films*, 2001, **393**, 109-113.
50. Y. Shirota and H. Kageyama, *Chem Rev*, 2007, **107**, 953-1010.
51. Y. Wang, S. Ge, M. Rafailovich, J. Sokolov, Y. Zou, H. Ade, J. Luning, A. Lustiger and G. Marom, *Macromolecules*, 2005, **38**, 2022-2022.
52. S. G. K. Jean-Michel Andanson, *Macromol. Symp.*, 2008, **265**, 195-204.
53. M. J. Frisch, *Chem Listy*, 2006, **100**, A9-A9.
54. M. C. Scharber, D. Wuhlbacher, M. Koppe, P. Denk, C. Waldauf, A. J. Heeger and C. L. Brabec, *Adv Mater*, 2006, **18**, 789-794.
55. S. J. Jo, C. S. Kim, J. B. Kim, S. Y. Ryu, J. H. Noh, H. K. Baik, Y. S. Kim and S. J. Lee, *J Appl Phys*, 2008, **103**,1-4.
56. M. P. de Jong, L. J. van IJzendoorn and M. J. A. de Voigt, *Appl Phys Lett*, 2000, **77**, 2255-2257.
57. K. W. Wong, H. L. Yip, Y. Luo, K. Y. Wong, W. M. Lau, K. H. Low, H. F. Chow, Z. Q. Gao, W. L. Yeung and C. C. Chang, *Appl Phys Lett*, 2002, **80**, 2788-2790.
58. C. H. Chang and S. A. Chen, *Appl Phys Lett*, 2007, **91,** 1-3.
59. S. T. Lee, Z. Q. Gao and L. S. Hung, *Appl Phys Lett*, 1999, **75**, 1404-1406.

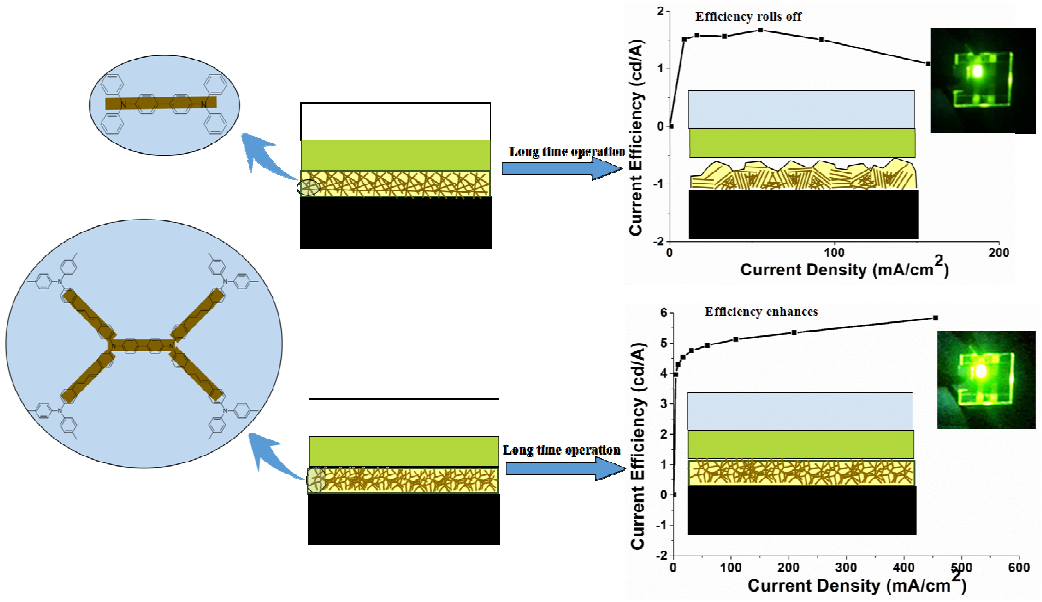

TPD(BTPA)$_4$ can improve the stability of OLED operated with high current and can achieve the one of the highest CE_{max} (5.83 cd A^{-1}) compared with reported small molecular (Mw<6000) HTMs in OLEDs with identical structure no mater solution processing or vacuum deposition.